Diffraction efficiency of reflective metallic gratings operating in the THz range

Alexander Cuadrado*,[1] , M. Fernández-Rodríguez[2] , Luis Miguel Sanchez-Brea[3] , Gonzalo García-Lozano[2], Guillermo Mercant[2] , Mª Carmen Torquemada[2] , Javier Alda[4] , Luis M. González[2], Tomás Belenguer[2] .

***Abstract*—Far infrared spectrometers have a prominent role to play in future space missions devoted to unveiling the obscure universe. Diffraction gratings are the heart of these instruments that, when operating in the range of a few THz, shall cover a wide spectral range providing the highest resolution and efficiency, generally for only a single polarization, within the specified spectral range. This contribution describes the optimization of the diffraction efficiency of the first diffractive order for a blazed metallic grating working at a large angle of incidence. Since the grating period is of the same order of magnitude as the wavelength, it is necessary to approach the design by solving Maxwell's equations rigorously using computational electromagnetism. We have applied the Rigorous Coupled-Wave Analysis and the Finite Element Methods to simulate the performance of the grating. This analysis provides relevant hints for the selection of the period, and the blaze and slant angles of the grating. A metallic blazed grating has been fabricated on aluminum and its topography has been characterized to determine the discrepancies with respect to the nominal values. The fabricated profile has been simulated to obtain the expected results in efficiency in comparison with the ideal case. This analysis provides guidance for improved manufacturing processes and experimental verification.**

***Keywords*—Terahertz, Far-IR optics, IR spectrometer, diffraction gratings, diffraction efficiency, computational electromagnetism.**

I. Introduction

The desire to learn more about the universe has consistently propelled the advancement of space instrumentation. The latest giant space telescopes launched into space, such as the Hubble [1] or the James Webb [2], with their onboard instruments, are examples of how technology is essential for observing and analyzing radiation that comes from space. With these tools, astronomers can study the origin and evolution of stars and galaxies, the composition of large masses of intergalactic dust, the development of planetary systems, and even inferring the habitability of some distant planet.

It is a fact that the longer the operating wavelength of an instrument, the less the effect of cosmic dust interference on the transmission of radiation, making it possible to detect light from more distant emitters. In the same way, the radiation arriving from a long distance in time and space tends to redshift, meaning that the wavelength of interest becomes longer. Measurements in the infrared wavelength domain allow direct assessment of the physical state and energy balance of cool matter in space. Previous infrared missions revealed significant information about the obscured universe but were hampered by limited sensitivity. Therefore, developing far-infrared instrumentation is a sure bet that will serve as a basis for future space missions. A future observatory would be, as was envisioned in the Space Infrared Telescope for Cosmology and Astrophysics mission (SPICA) [3], a large telescope with instruments including a far-infrared spectrometer. The spectrometer heart would be a diffraction grating capable of withstanding the demanding conditions of space. The design of this type of gratings is dictated by many factors, being the most important the resolution, efficiency, and spectral range. To achieve low total diffraction angles, leading to compact optical designs of moderate dimensions, it is often necessary to design identical modules for different spectral ranges, each with a dedicated grating design. Obviously, the diffraction grating design and the knowledge of its behavior under operating conditions become decisive factors in the design of the instrument [4].

In this contribution, we present the design process of a reflective diffraction grating operating in the range from 70 to 114 microns (2,6 - 4 THz). This spectral range is within the working spectral range of SPICA spectrometer (34-230 microns), where the diffraction efficiency should be over 65% to meet SPICA sensitivity requirements. The grating has a period very close to the wavelength of the incident radiation and becomes a sub-wavelength grating [5]. This means that even though the angle of incidence is large, a few diffractive orders will be reflected from the grating. Moreover, under conditions of fixed incidence, Wood's anomalies become evident as one approaches wavelengths where a particular diffractive order is poised to vanish. In these situations, the power budget among orders is strongly modified [6], [7]. Furthermore, the blazed geometry with a sawtooth profile generates different responses for the TM (transversal magnetic) and TE (transversal electric) polarization components. All this together challenges the grating design and requires the use of computational electromagnetism tools to properly model the spectral response of the grating, in terms of its characteristic parameters. The Rigorous Coupled-Wave Analysis (RCWA) is very well suited for the study of periodic structures and it becomes a straightforward election in our case [8]–[10]. In

[*] Corresponding author: alexander.cuadrado@urjc.es

[1] Escuela de Ciencias Experimentales y Tecnología, Universidad Rey Juan Carlos, 28933, Madrid, Spain.

[2] Departamento de Óptica Espacial. Instituto Nacional de Técnica Aeroespacial (INTA), Carretera de Ajalvir Km. 4, Torrejón de Ardoz, Madrid, 28850, Spain.

[3] Applied Optics Complutense Group. Facultad de Ciencias Físicas. Universidad Complutense de Madrid, 28040, Madrid, Spain.

[4] Applied Optics Complutense Group. Facultad de Óptica y Optometría, Universidad Complutense de Madrid, 28037, Madrid, Spain.

this work, we have also simulated our grating using a Finite Element Method (FEM). Previous analysis comparing these two approaches [11] shifts our confidence towards the FEM simulator.

After reviewing the fundamentals of blazed diffraction gratings in section II, we have used numerical techniques in section III to better understand how the geometric parameters of the blazed grating determine its diffractive performance. Section IV presents a diffraction grating fabricated with geometric parameters that comply with the given specifications. The results show how some imperfections in the fabrication may strongly reduce the diffractive efficiency expected for an ideal shape. Finally, section V summarizes the main findings of this contribution.

II. Fundamentals of Reflective Metallic Gratings for THz Spectroscopy

Figure 1 shows a schematic layout of our spectrometer. Its input is defined by a slit placed at the object focal plane of the collimator subsystem. The collimated beam reaches the grating and the diffracted light is collected and focused by the concave mirror on the image plane. This spectrometer uses a large angle of incidence on the diffraction grating allowing for a more compact optical layout. The grating itself benefits from a blazed design to increase the energy reflected to the diffractive order of interest. These conditions favor the reflection of the TM component of light. Therefore, we pay our attention to the diffractive efficiency of the TM mode. As far as we know, our design is the first reflective blazed diffraction grating reported to work at this terahertz range, operating only in the first order. Many other gratings, working at different wavelengths, have been reported; for example, high efficiency slanted grating for RGB (red-green-blue) bands [12], an enhanced diffraction efficiency for non-polarized lasers at 1064 nm with a rectangular three-layer multilayer grating [13]. At the terahertz range, a diffractive binary grating was used in a photoconductive antenna for time-domain spectroscopy [14]. In the same spectral range, two Littrow configuration gratings were used as part of the FIFI_LS spectrometer for the SOFIA airborne observatory, operating at first and second orders [15], [16], and also at PACS instrument on Herschel ($55-210\mu$m) that operates in the first three orders, covering the entire spectral range with a single diffraction grating showing a diffraction efficiency of 60% [17]. In our case, the proposed grating works in a shorter spectral range for a single diffraction order, but its efficiency reaches values larger than 90% for the ideal design, and greater than 65% for the fabricated grating, within our spectral range of interest .

The metallic grating analyzed in this paper has a period, d, and a blazed profile, with a blaze angle γ and a slant angle β as shown in Fig. 2. The spectrometer works with an angle of incidence on the grating that is $\theta_{\rm inc}$. In these conditions, the angle of the diffracted order m, θ_m, follows the well known relation [6]

$$d(\sin\theta_{\rm inc}+\sin\theta_m)=m\lambda, \tag{1}$$

where θ_m and $\theta_{\rm inc}$ refer to the normal to the horizontal plane where the period of the grating is defined, d (see Fig. 2).

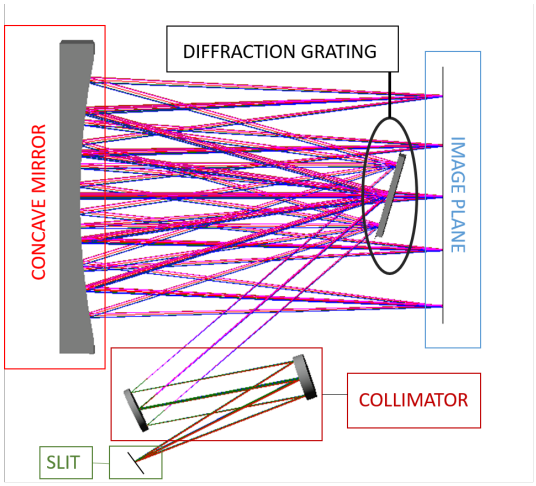

Fig. 1. Graphical layout of the far infrared spectrometer where the metallic grating is included.

From Eq. (1) we can obtain the angular location of the orders,

$$\theta_m=\sin^{-1}\left(\frac{m\lambda}{d}-\sin\theta_{\rm inc}\right), \tag{2}$$

where the non-evanescent orders are those that fulfill

$$\frac{d}{\lambda}(\sin\theta_{\rm inc}-1)<m<\frac{d}{\lambda}(\sin\theta_{\rm inc}+1). \tag{3}$$

Equation (2) also determines the angular extent or total diffraction angle, $\Delta\theta_m$, of the diffractive order m, for a spectral range between $\lambda_{\rm min}$ and $\lambda_{\rm max}$, that is an important parameter in the design of the whole spectrometer.

$$\Delta\theta_m=\left|\sin^{-1}\left(\frac{m\lambda_{\rm max}}{d}-\sin\theta_{\rm inc}\right)-\sin^{-1}\left(\frac{m\lambda_{\rm min}}{d}-\sin\theta_{\rm inc}\right)\right|. \tag{4}$$

TABLE I. Initial specifications for the grating.

Variable	Value
Spectral range	$[70-114]\mu$m
Diffraction order	1
Polarization	Transversal Magnetic (TM)
Total diffraction angle, $\Delta\theta_m$	$30^\circ-40^\circ$
Diffraction efficiency, DE, η	$>65\%$
Angle of incidence, $\theta_{\rm inc}$	57°
Spectral resolution ($\lambda/\Delta\lambda$)	200

In our case, the initial specifications of the grating are given in table I [4]. The grating period d has a value similar to λ, which limits the number of allowed diffraction orders to $m=0,1$, and 2. In this situation, the diffraction efficiency, η, needs to be evaluated using computational electromagnetism packages. This analysis, as well as the previous results, reveals some anomalies in the energy distribution between orders for this type of grating [6], [7]. These anomalies appear around the spectral location where a given order is no longer possible. Considering Eq. (1), we can obtain the cut-off wavelengths as

$$\lambda_{m,{\rm cut-off}}=\frac{d(\sin\theta_{\rm inc}\pm1)}{m}, \tag{5}$$

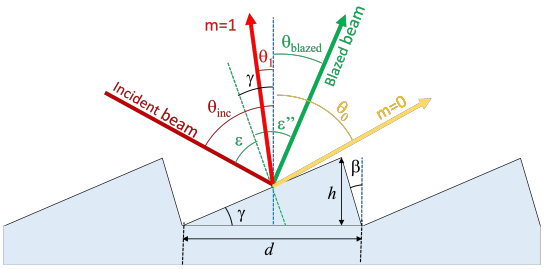

Fig. 2. The metallic grating has a period d, a height h, and a triangular profile characterized by the blaze angle, γ, and the slant angle, β. The incident beam subtends an angle $\theta_{\rm inc}$ with respect to the normal to the grating plane (horizontal), and an angle ε with respect to the normal of the blazed surface. The orders of diffraction reflect with an angle given by equation (1). At the same time, the mirror reflection at the blazed surface subtends an angle ε'' with respect to the normal to this surface, following the mirror reflection law: $\varepsilon'' = -\varepsilon$. We have represented the incident beam, the diffractive orders with $m = 0$ and $m = 1$, and the mirror reflection at the blazed surface that we name as "blazed beam", with angles θ_0, θ_1, and $\theta_{\rm blazed}$, respectively. In this figure, we have followed the sign convention of the geometrical optics, meaning that $\theta_{\rm inc}$, θ_1, and ε are positive, meanwhile, θ_0, $\theta_{\rm blazed}$, and ε'' are negative. Angles γ and β are considered positive.

where m is the diffraction order and the $\pm$ sign corresponds to an angle of diffraction equal to $+90°$ and $-90°$, respectively. Figure 3 shows the cut-off wavelength for orders $m = 1, 2$ and 3. We have also represented the spectral range of interest $[70 - 114]\mu$m as horizontal dashed lines. Order $m = 3$ never happens for the analyzed interval in d. However, within the spectral range of interest, two anomalies occur at $d_{\rm min} = 62\mu$m and $d_{\rm max} = 76.1\mu$m. They affect the first and second orders, respectively, disturbing the energy distribution among orders. As a consequence of this analysis, we may establish a design condition as

$$d_{\rm min} < d < d_{\rm max}. \tag{6}$$

Even though the modes actually disappear at these two limiting values in d, the spectral width of the anomaly should require some safeguards bands in the value of d on both sides.

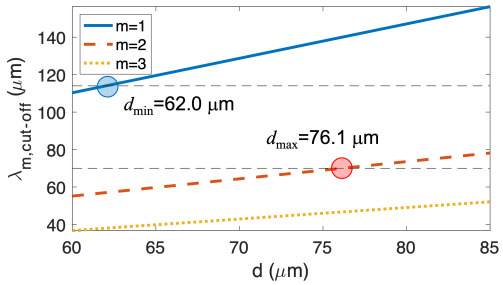

Fig. 3. Value of $\lambda_{m,{\rm cut-off}}$ (Eq. (5)) as a function of the grating period, d. The horizontal dashed lines represent the spectral interval of interest. The third order never appear, and the second and first diffractive orders dissapear at $d = 76.1\mu$m, and $d = 62.0\mu$m, respectively.

The response of sub-wavelength blazed gratings depends on the polarization of the incoming radiation. TE and TM components behave differently, with the height to width aspect ratio, h/d, being one of the main factors responsible for this difference [18]. There is also a strong dependence on the polarizing properties of metal gratings on the period/wavelength relationship. Periods comparable with the wavelength induce an anomalous high transmission of the TE component of light, which has already been used to design metal-stripe polarizers [19].

The advantage of a blazed grating is that the amount of energy diffracted at a given order, in our case $m = 1$, is enhanced. As we can see in Fig. 2, the angle of incidence with respect to the grating, $\theta_{\rm inc}$, becomes an angle of incidence with respect to the blazed surface when referred to the normal to this surface, ε. Geometrically, this angle of incidence is given as $\varepsilon = \theta_{\rm inc} - \gamma$. The reflection law can be used to obtain the direction of the mirror reflection – blazed beam in Fig. 2 – with respect to the normal to the grating, that is $\theta_{\rm blazed} = 2\gamma - \theta_{\rm inc}$.

The operating temperature in space determines the material used to manufacture the diffraction grating. Aluminum 6061T651 is our preferred option as it is easy to mechanize and remains corrosion-resistant even when the surface is abraded. From the electromagnetic point of view, the Drude model [20] serves to estimate the optical constant of the metal in the far infrared region that is used in the calculation of the reflectivity of the material [21].

The detailed analysis of all the involved parameters should be made using simulation tools that consider not only the application of the grating equation (Eq. (1)) but also the dependence of the diffraction efficiency with the material characteristics and the blazed and slant angles, γ and β, respectively. As shown in Fig. 2, the slant angle serves to describe the fabrication limits when manufacturing a perfect sawtooth profile ($\beta = 0°$).

III. Modeling and Simulation of THz Metallic Gratings

The design of the grating is defined by the spectrometer specifications and the principles explained in section II. Next, we have numerically evaluated the performance of the device to make a fine tuning of its geometrical parameters. This has been done using two approaches in computational electromagnetism: the Rigorous Coupled-Wave Analysis, and the Finite Element Model.

RCWA is an implementation of the Fourier modal method (FMM) [22] for simulating electromagnetic propagation. It provides a numerical solution to Maxwell's equations for a periodic structure that lies between two homogeneous linear media [10], which is the case treated in this contribution. The grating profile is divided into a number of slices, parallel to the surface, where the index modulation remains periodic. Each slice is treated as a thin diffraction grating, where permittivity is expanded as a Fourier series. The number of terms, or orders, in the Fourier expansion of the permittivity also determines the reliability of the results. The minimum number of orders is related to the grating period and wavelength as $2d/\lambda$. Generally, a structure with several slices requires more orders, and metals require lots of evanescent orders to achieve accurate results. A small number of slices, or orders in the

Fourier expansion, will not faithfully represent the shape of the profile, or the permittivity at each slice, respectively, generating inaccurate results. On the contrary, by increasing the number of slices and orders, the structure is better reproduced at a cost of a large processing time and computational resources. An adequate trade-off between accuracy and computational effort should be applied to obtain convergence in the values of the diffraction efficiency. In this paper, we have used two RCWA solvers: GSolver (Grating Solver Development Company, UT, USA), and S^4 (Stanford Stratified Structure Solver, Stanford University, CA, USA) [23].

The FEM approach solves a set of partial differential equations – in our case, the Maxwell equations – on a collection of finite elements that are obtained through meshing. The method applies boundary value conditions and generates a set of linear equations that are numerically solved to find a solution. The accuracy of FEM strongly depends on the type of mesh used to tessellate the domain of interest [11]. In computational electromagnetism using FEM, the meshing has to be a fraction of λ. This fact makes FEM very demanding in computational resources, especially memory allocation capabilities. To properly simulate the metallic diffraction grating, we apply periodic boundary conditions and place the source and listening ports at the correct angular location to collect the radiation of the diffracted orders and evaluate their diffractive efficiency, η_m. The method has already been used as a numerical solver for the analysis of diffraction gratings [24]. In this paper, we have used Comsol Multiphysics (Comsol AB, Stockholm, Sweden) as an implementation of the FEM for computational electromagnetism.

Both RCWA and FEM generate reliable values of the diffraction efficiency of the grating at the available orders of diffraction and the near field maps for the electromagnetic variables of interest (electric and magnetic fields, Poynting vector, energy dissipation, etc.). These results are analyzed in this section to soundly evaluate the grating performance. All the simulations have been made for a perfect structure with geometrical parameters varying according to the needs of the design. The initial conditions for the design are given in table I. In Fig. 4 we show the diffractive efficiency for orders $m = 0$ and $m = 1$ for an aluminum blazed grating having a period $d = 76\mu$m and a blaze angle $\gamma = 23.5°$. We can see that the FEM solution calculated with Comsol Multiphysics provides higher values of η_1 than RCWA, but this difference decreases as the number of slices and terms in the Fourier expansion increases.

Considering the data shown in Fig. 3 of section II, and under the conditions given in table I, we have simulated the spectral diffraction efficiency at the diffractive order of interest, $m = 1$, for two values of the grating period, $d = 70\mu$m and $d = 76\mu$m, for a slanted angle $\beta = 0°$, and also as a function of it to evaluate fabrication issues [25].

Figure 5 represents the results of the calculated spectral efficiency for a blazed aluminum grating having a period $d = 70\mu$m, as a map (in Fig. 5.a) in terms of λ and γ. We can see in the color map that this efficiency is much higher than the minimum specification of 65% (see Tab. I) for the whole spectrum and blaze angle values. In Fig. 5.b we have

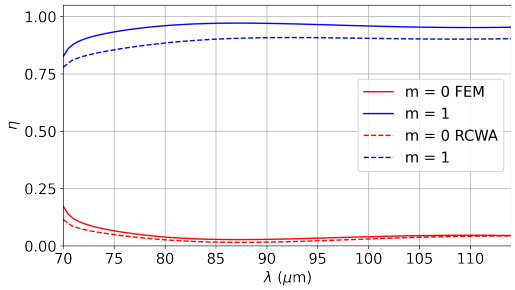

Fig. 4. Spectral diffractive efficiency, η, for order $m = 0$ and $m = 1$ for a blazed aluminum grating with $d = 76\mu$m, and $\gamma = 23.5°$. The solid lines represent the FEM solution, and the dashed lines are for the RCWA approach.

represented three quality parameters of the spectral efficiency. The standard deviation, σ, measures the flatness of the curve, the mean efficiency, $\langle\eta_1\rangle$, describes the average value of the diffraction efficiency within the spectral range of interest for order $m = 1$, and the minimum efficiency, $\eta_{1,\min}$, reports the minimum value of the diffraction efficiency. From this figure, we can extract the values of the blaze angle that best behave. This means that the lowest value in σ occurs at $\gamma = 24°$, and the highest value in mean and minimum efficiency, $\gamma = 26°$ and $\gamma = 23.5°$, respectively. The spectral efficiencies for these optimum values are represented in Fig. 5.c.

Some constraints imposed by the spectrometer requirements, such as the volume and mass, force us to move the value of the grating period to $d = 76\mu$m. The mass and volume limitations require the use of high angle incident radiation. In this case, the angle of incidence with which the radiation falls on the diffraction grating must be $\theta_{\text{inc}} = 57°$. This value affects and conditions fundamental parameters such as the total diffraction angle, $\Delta\theta$, already defined in Eq. (4). This parameter should be between 30-40º to avoid a large aperture of the camera, increasing the size and weight of the spectrometer. On the other hand, the value of $\Delta\theta_1$ decreases when d increases, so a larger value of d would ease compliance with the specifications (see Tab. I). As a matter of fact, the values of the total diffraction angle are $\Delta\theta_1 = 42.9°$ and $36.7°$, for $d = 70\mu$m and 76μm, respectively. Therefore, $\Delta\theta_1$ for a grating of period $d = 70\mu$m would be out of specifications.

The results of the diffraction efficiency for $d = 76\mu$m are given in Fig. 6. In this figure we can see how the diffraction anomalies begin to happen, as predicted from the analysis of the cut-off wavelength (see Fig. 3), because we are very close to $d = 76.1\mu$m where the order $m = 2$ disappears. However, the minimum efficiency is well above 65% for most of the blaze angle range, passing the spectrometer requirements. Even more, when calculating the behavior of the grating as a function of the slant angle, β for a fixed value of $\gamma = 24°$, we find that the anomaly is removed and the efficiency remains above 90% in the whole spectral range (see Figure 7). In other words, considering a slant angle of 5 or 10 degrees would result in better spectral efficiency than considering a sawtooth profile. Geometrically, increasing the slant angle decreases the value of h (see Fig. 2).

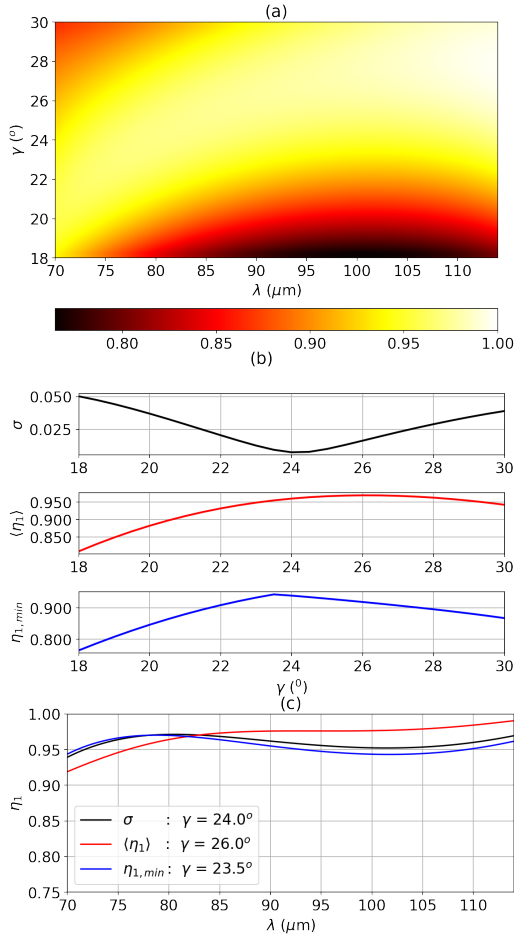

Fig. 5. Results for $d = 70\mu m$ obtained using Comsol Multiphysics. (a) Map of the spectral diffractive efficiency, η_m at $m = 1$ when the blazed angle, γ, varies from 18° to 30°. (b) Dependence of the standard deviation, σ, the averaged efficiency, $\langle\eta_1\rangle$, and the minimum efficiency, $\eta_{1,\min}$, as a function of the blaze angle, γ. (c) Spectral efficiency, η_1 for the three optimum values of γ detected in subplot (b).

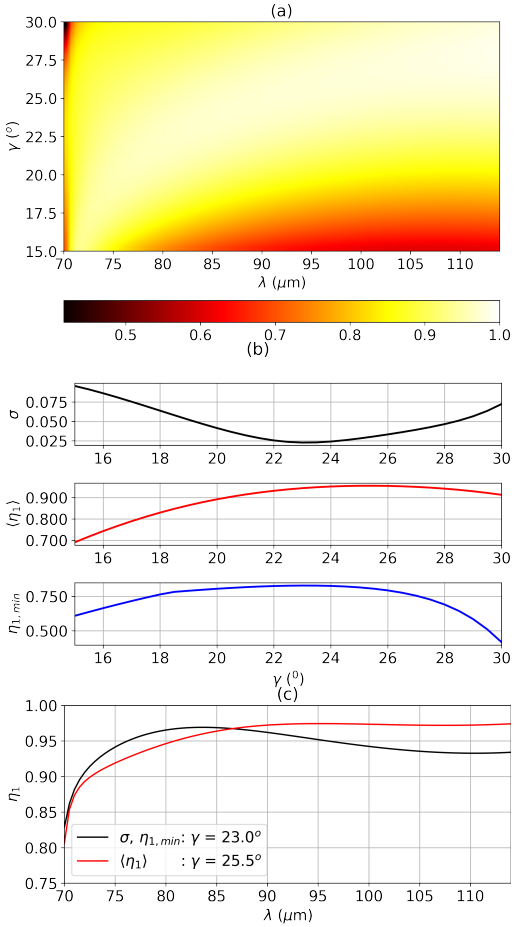

Fig. 6. Results for $d = 76\mu$m obtained using Comsol Multiphysics. (a) Map of the spectral diffractive efficiency, η_m at $m = 1$ when the blazed angle, γ, varies from 18° to 30°. (b) Dependence of the standard deviation, σ, the averaged efficiency, $\langle\eta_1\rangle$, and the minimum efficiency, $\eta_{1,\min}$, as a function of the blaze angle, γ. (c) Spectral efficiency, η_1 for the two optimum values of γ detected in subplot (b).

IV. Fabrication of THz metallic gratings

The manufacturing process distorts the geometry of the theoretical design and generates unavoidable discrepancies between the ideal profile and the actual one. These differences need to be quantified in terms of their influence on the performance of the device, and we will do so by applying the same simulation techniques that we have used during the design.

In our case, we have fabricated a grating on a metallic substrate, specifically aluminum 6061T651, which is the most suitable material for space applications due to its mechanical and thermal properties. Obviously, the similarities between the fabricated and designed profiles depend on the manufacturing technique used. A blazed aluminum diffraction grating with sawtooth-shaped geometry and a total area of 54×40 mm^2 has been manufactured by micro-milling techniques using the specifications given in table II. A high-precision 3-axis machining center equipped with a high-speed and high-rigidity head was used. The grating was engraved on an inclined surface using a custom-made high-precision rotating cutting tool to remove material Once fabricated, the characterization of its morphology allows a detailed analysis of how the manufacturing defects modify the diffraction efficiency. Figure 8.a shows an optical microscopy image in which the sawtooth grooves of the diffraction grating can be seen. A scanning electron microscopy (SEM) image is shown in Figure 8.b, where the grating border shows some edge effects caused by the tool used to mechanize the device. To prevent undesired effects on diffraction efficiency, the terahertz radiation shall not reach the border region. The period extracted from these measurements slightly differs from the nominal values. Figure 9.a shows an image acquired by confocal microscopy. It is clear that the sawtooth profile contains fabrication defects and is not like the ideal one that was modeled. In Figure 9.b, the inhomogeneous profile is observed and the period is divided into four repeated portions. Region A is a flat part at the bottom of the profile that occupies between 20% and 30%

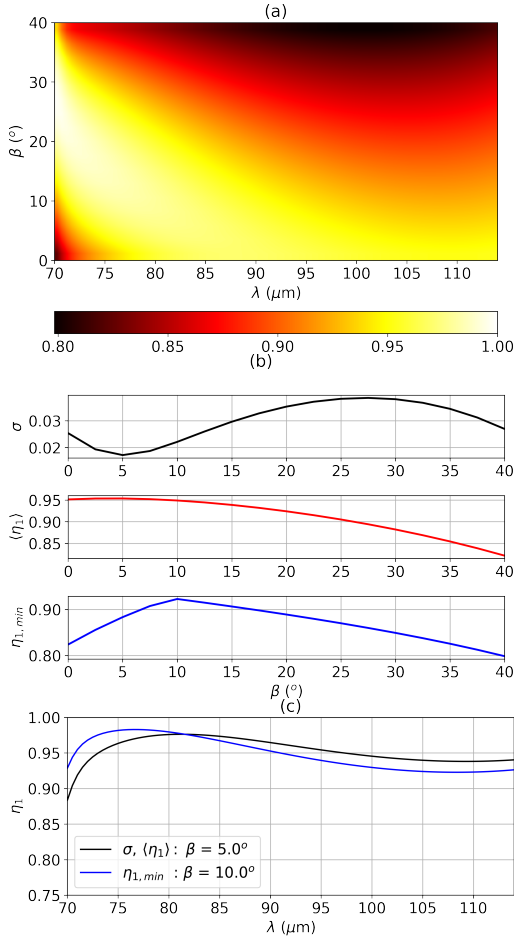

Fig. 7. Results for $d = 76\mu m$ and $\gamma = 24°$ obtained using Comsol Multiphysics. (a) Map of the spectral diffractive efficiency, η_m at $m = 1$ when the slant angle, β, varies from $0°$ to $40°$. (b) Dependence of the standard deviation, σ, the averaged efficiency, $\langle\eta_1\rangle$, and the minimum efficiency, $\eta_{1,\min}$, as a function of the slant angle, β. (c) Spectral efficiency, η_1 for the two optimum values of β detected in subplot (b).

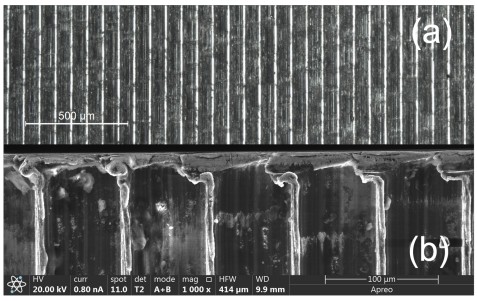

Fig. 8. (a) Visual inspection of the diffraction grating obtained with an optical microscope. (b) Detail of the edges of the micromachined diffraction grating obtained by scanning electron microscopy. The borders of the metallic piece present aluminum material accumulations.

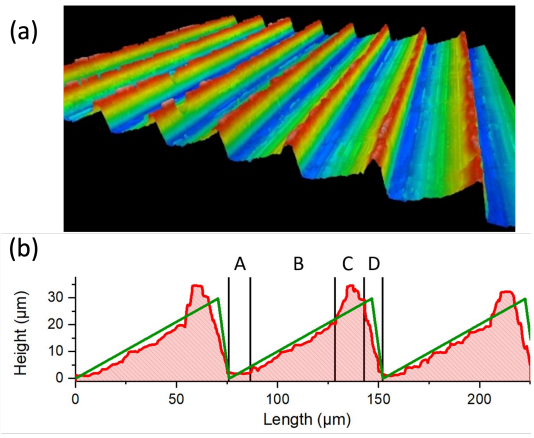

Fig. 9. Geometrical characterization of the micromachined diffraction grating. (a) Topography obtained from confocal microscopy. (b) Detail of the measured profile showing four regions within a period: A) is a flat region, B) represents the blazed portion of the period, C) corresponds to the shape of the peak of the profile, and D) is the portion corresponding to the slant angle. This structure repeats along the whole topography. The nominal geometry (see Table II) is represented as a green line.

of the period, B corresponds with the blazed portion, region C is the top part of the profile that shows an important variation among periods, and finally, D is the slant portion that reveals the lack of verticality of the sawtooth profile, with $\beta = 20°$. The green line in this figure represents the nominal geometry (see Table II). We can see how region C is the one that departs the most from the ideal topography.

After manufacturing the grating, we can conclude that discrepancies between the designed ideal profile and the real manufactured exist. The average values of the main sawtooth parameters measured along the entire area are summarized in table II compared with the nominal values of the ideal modeled profile. From the measured topography, we have obtained the grating period by determining the distance between two consecutive maxima of the profile. These period values have been averaged on several small areas (0.33×4.09 mm^2) along the grating surface. The same has been done with the blazed angle, γ, and the height, h. Figure 10 shows the histogram of the period, the height, and the blaze angle. They show a Gaussian distribution that serves to determine the average and the error presented in the last column of table II. All the values of the geometry are within specifications, except the slant angle that shows a larger value than expected. On other hand, discrepancies between the manufactured profiles and the ideal ones have to be taken into account, that is, the presence of a flat zone, a slant angle and the non-uniformity at the blazed side. Along the fabrication process, we observed that the tool used in the micro-milling was not symmetrically perfect, which produced defects when rotating. Therefore, the manufacturing could be improved with machining strategies that minimize the effect of the lack of symmetry of the micro-machined milling tool.

The results from the topographic measurements have been used to evaluate the response of the fabricated grating. This simulation has required a large number of cells to faithfully reproduce the actual profile. In our calculation we have used the measured topography of 8 periods of the fabricated grat-

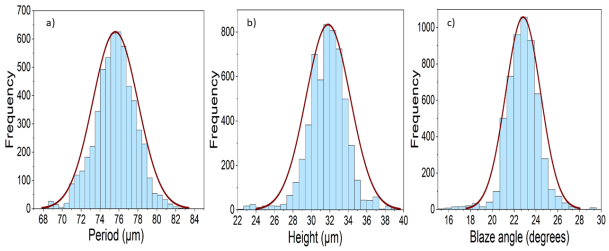

Fig. 10. Geometrical characterization of the micro-machined diffraction grating. Statistics of the geometrical parameters along the diffraction grating surface.(a) Average period value $d = 75 \pm 2\mu$m. (b) Average height value $h = 32 \pm 2\mu$m (c) Average Blaze angle $\gamma = 23 \pm 2$ degrees.

TABLE II. NOMINAL AND REAL PARAMETERS.

Parameter	Nominal	Real
$d(\mu\text{m})$	76	75 ± 2
$h(\mu\text{m})$	31	32 ± 2
Blaze, $\gamma(^\circ)$	$23,5$	23 ± 2
Slant, $\beta(^\circ)$	10	20

ing. This 8-period unit cell has been repeated using periodic boundary conditions at both sides. Fig. 11.a shows the diffractive efficiency for the real profile (red line). We have also plotted the response to the nominal profile (green plot), and the efficiency for an averaged profile obtained from the topographic measurements (in blue). We can see how the large discrepancies between the fabricated and nominal gratings generate a strong decrease in efficiency. At the same time, the simulations using an averaged profile with flat surfaces reproduces very well the response obtained for the actual profile, without demanding fine meshing of the topography. Even though the fabricated topography largely departs from the nominal, the calculated efficiency is above 65% for the whole spectral range. The simulation also provides electromagnetic field maps. Fig. 11.b shows the magnetic field where we can clearly see how the periods behave differently, depending on the individual shape, with strong variation in the intersection of regions C and D of the topography (see Fig. 9) The red arrow represents the incident direction and the black one points towards the diffractive order $m = 1$.

V. CONCLUSIONS

In this contribution, we present an optimization methodology for the design of metallic blazed diffraction grating for its use in the high-frequency THz band, $\lambda \in [70, 114]\mu$m, for space exploration applications. The analysis of the blazed diffraction grating equation, that reveals Wood's anomalies when the wavelength approaches the cut-off wavelength of the given order, defines an interval for the grating period that locates the diffractive order of interest away from these anomalies. A detailed numerical analysis has been made using two main computational electromagnetism methods: RCWA and FEM. Both of them produce similar values of efficiency (above 90%) and can be used to optimize the performance of the grating by changing the geometrical parameters (period, blaze, and slant angles). The final design should take into

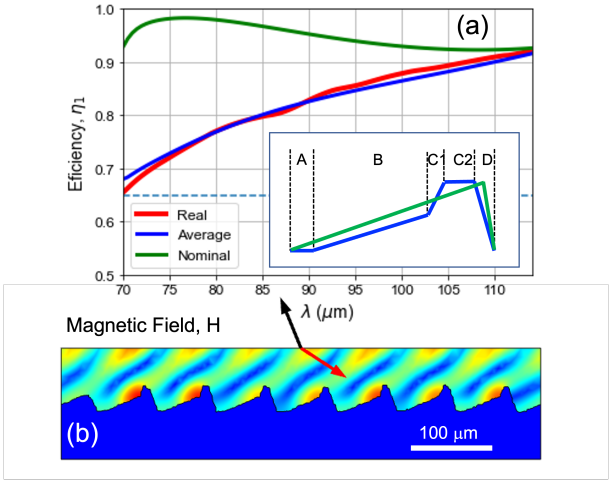

Fig. 11. (a) Diffractive efficiency calculated using the measured topography of 8 periods of the fabricated grating (red), an average of this topography approached with flat surfaces (blue) and the nominal profile (green) described in table II. In the inset we have plotted the nominal and the averaged profile obtained from the confocal measurements. This averaged profile has the following parameters: the A region is 4.6 μm long, the blazed region B has an angle $\gamma = 20.8^\circ$, the C region is divided in two: the C1 portion is a blazed surface with an angle of 67.3°, and flat portion (C2) 5.82 μm long, finally, portion D has a slant angle $\beta = 20.9^\circ$ (b). Map of the magnetic field in the near-field region of the grating. The red arrow indicates the direction of the incident beam, and the black arrow points toward the direction of the $m = 1$ diffractive order.

account the fabrication limitations and the fulfillment of the specifications. Therefore, even though a grating period of $d = 70\mu$m behaves quite well in terms of homogeneity and the absolute value of the diffractive efficiency, we moved to a value of $d = 76\mu$m that produces a smaller total diffraction angle, $\Delta\theta_1$. The closeness of this value to the cut-off wavelength of the second diffractive order has generated a sudden decrease in diffractive efficiency around $\lambda = 70\mu$m. Fortunately, when analyzing the role of the slant angle, β, the calculated efficiency increases, compensating the effect of the diffractive anomalies.

After considering all these issues in the design, we have fabricated an aluminum blazed grating with a period $d = 76\mu$m, a blazed angle $\gamma = 23.5^\circ$ and a slant angle of around $\beta = 10^\circ$. This grating has been fabricated by micromachining. The manufactured relief has been geometrically characterized by confocal and scanning electron microscopy. This profile measurement helps to obtain an averaged profile that uses flat, but blazed and slanted, surfaces. The actual and averaged geometry has been also included in the simulations and the diffraction efficiency has been evaluated with the computational electromagnetism packages already employed in the design process. We have seen that the memory allocation requirements have been eased by considering the flat surface geometry obtained from the profile characterization. Even though the efficiency dramatically drops from the nominal case, it still remains above specifications with values greater than 65%. Next step will be the experimental verification of the grating diffraction efficiency. For this purpose, quantum

cascade lasers emitting at the range of interest could be a first choice. The set-up should include off-axis parabolic mirrors, and a pyroelectric detector, properly arranged to provide an accurate measurement of the involved diffraction angles and signals.

ACKNOWLEDGMENTS

G. García-Lozano, G. Mercant, M Fernández, M.C. Torquemada, L. González, and T. Belenguer thank to the Spanish Ministerio de Ciencia y Universidades for funding this activity under grant PID2019-105552RB-C42. J. Alda and L. M. Sanchez-Brea acknowledge funding from Plan Nacional de Investigación of the Ministerio de Ciencia e Innovación through project PID2019-105918GB-I00. A. Cuadrado thanks the support from Proyectos de I+D para jóvenes investigadores de la Universidad Rey Juan Carlos, funded by Comunidad de Madrid, Código 2022/00156/025, REF:M2742.

REFERENCES

[1] NASA, "Hubble space telescope," https://www.nasa.gov/mission_pages/hubble/main/index.html, [Accessed 2023]. [Online]. Available: .https://www.nasa.gov/mission_pages/hubble/main/index.html.

[2] ——, "James webb space telescope," https://www.jwst.nasa.gov/index.html, [Accessed 2023]. [Online]. Available: https://www.jwst.nasa.gov/index.html.

[3] P. R. Roelfsema, H. Shibai, L. Armus, D. Arrazola, M. Audard, M. D. Audley, C. Bradford, I. Charles, P. Dieleman, Y. Doi, and et al., "Spica—a large cryogenic infrared space telescope: Unveiling the obscured universe," *Publications of the Astronomical Society of Australia*, vol. 35, p. e030, 2018.

[4] D. Arrazola, M. Fernández, L. M. G. Fernández, T. Belenguer, W. Jellema, G. Rafael, J. Torres, G. de Lange, J. Evers, M. Eggens, and et al., "The optical design of a far infrared spectrometer for SPICA: grating modules evaluation," in *Millimeter, Submillimeter, and Far-Infrared Detectors and Instrumentation for Astronomy IX*, J. Zmuidzinas and J.-R. Gao, Eds., vol. 10708, International Society for Optics and Photonics. SPIE, 2018, p. 107083G. [Online]. Available: https://doi.org/10.1117/12.2315971

[5] M. A. Golub and A. A. Friesem, "Analytic design and solutions for resonance domain diffractive optical elements," *J. Opt. Soc. Am. A*, vol. 24, no. 3, pp. 687–695, Mar 2007. [Online]. Available: https://opg.optica.org/josaa/abstract.cfm?URI=josaa-24-3-687

[6] E. G. Loewen and E. Popov, *Diffraction gratings and applications*. CRC Press, 2017.

[7] F. Falco, T. Tamir, and K. M. Leung, "Grating diffraction and wood's anomalies at two-dimensionally periodic impedance surfaces," *J. Opt. Soc. Am. A*, vol. 21, no. 9, pp. 1621–1634, Sep 2004. [Online]. Available: https://opg.optica.org/josaa/abstract.cfm?URI=josaa-21-9-1621

[8] M. G. Moharam and T. K. Gaylord, "Rigorous coupled-wave analysis of planar-grating diffraction," *J. Opt. Soc. Am.*, vol. 71, no. 7, pp. 811–818, Jul 1981. [Online]. Available: https://opg.optica.org/abstract.cfm?URI=josa-71-7-811

[9] ——, "Rigorous coupled-wave analysis of metallic surface-relief gratings," *J. Opt. Soc. Am. A*, vol. 3, no. 11, pp. 1780–1787, Nov 1986. [Online]. Available: https://opg.optica.org/josaa/abstract.cfm?URI=josaa-3-11-1780

[10] M. G. Moharam, E. B. Grann, D. A. Pommet, and T. K. Gaylord, "Formulation for stable and efficient implementation of the rigorous coupled-wave analysis of binary gratings," *J. Opt. Soc. Am. A*, vol. 12, no. 5, pp. 1068–1076, May 1995. [Online]. Available: https://opg.optica.org/josaa/abstract.cfm?URI=josaa-12-5-1068

[11] M. E. Solano, M. Faryad, A. Lakhtakia, and P. B. Monk, "Comparison of rigorous coupled-wave approach and finite element method for photovoltaic devices with periodically corrugated metallic backreflector," *J. Opt. Soc. Am. A*, vol. 31, no. 10, pp. 2275–2284, Oct 2014. [Online]. Available: https://opg.optica.org/josaa/abstract.cfm?URI=josaa-31-10-2275

[12] G. Jin, W. Liu, Z. Ye, W. Jia, Y. Xie, and C. Zhou, "High efficiency polarization-independent slanted grating for rgb bands," *IEEE Photonics Journal*, vol. 13, no. 4, pp. 1–8, Aug 2021.

[13] D. T. Cu, T. D. Pham, V. T. H. Le, M. C. Li, H. P. Chen, and C. C. Kuo, "Design of a high-efficiency multilayer dielectric diffraction grating with enhanced laser damage threshold," *Nanomaterials*, vol. 12, no. 12, 2022. [Online]. Available: https://www.mdpi.com/2079-4991/12/12/1952

[14] J. Y. Chia, K. Tantiwanichapan, R. Jintamethasawat, A. Sathukarn, W. Kusolthossakul, and N. Nuntawong, "A computational study on performance improvement of thz signal from a grating photoconductive antenna," *Photonics*, vol. 7, no. 4, 2020. [Online]. Available: https://www.mdpi.com/2304-6732/7/4/108

[15] W. Raab, A. Poglitsch, R. Klein, R. Hoenle, M. Schweizer, W. Viehhauser, N. Geis, R. Genzel, L. W. Looney, M. Hamidouche, and et al., "Characterizing the system performance of FIFI LS: the field-imaging far-infrared line spectrometer for SOFIA," in *Ground-based and Airborne Instrumentation for Astronomy*, I. S. McLean and M. Iye, Eds., vol. 6269, International Society for Optics and Photonics. SPIE, 2006, p. 62691G. [Online]. Available: https://doi.org/10.1117/12.671483

[16] L. W. Looney, N. Geis, R. Genzel, W. K. Park, A. Poglitsch, W. Raab, D. Rosenthal, A. Urban, and T. Henning, "Realizing 3D spectral imaging in the far-infrared: FIFI LS," in *Airborne Telescope Systems*, R. K. Melugin and H.-P. Roeser, Eds., vol. 4014, International Society for Optics and Photonics. SPIE, 2000, pp. 14 – 22. [Online]. Available: https://doi.org/10.1117/12.389112

[17] Poglitsch, A., Waelkens, C., Geis, N., Feuchtgruber, H., Vandenbussche, B., Rodriguez, L., Krause, O., Renotte, E., van Hoof, C., Saraceno, P., and et al., "The photodetector array camera and spectrometer (pacs) on the herschel space observatory*," *A&A*, vol. 518, p. L2, 2010. [Online]. Available: https://doi.org/10.1051/0004-6361/201014535

[18] G. Sridharan, V. Pramitha, and S. Bhattacharya, "Design and fabrication of lower aspect ratio sub-wavelength grating for polarization separation," in *International Conference on Fibre Optics and Photonics*. Optica Publishing Group, 2012, p. MPo.14. [Online]. Available: https://opg.optica.org/abstract.cfm?URI=Photonics-2012-MPo.14

[19] M. Honkanen, V. Kettunen, M. Kuittinen, J. Lautanen, J. Turunen, B. Schnabel, and F. Wyrowski, "Inverse metal-stripe polarizers," *Applied Physics B*, vol. 68, no. 1, pp. 81–85, 1999. [Online]. Available: https://doi.org/10.1007/s003400050590

[20] N. D. Mermin and N. W. Ashcroft, *Solid state physics*. Cengage Learning India, 2003.

[21] M. Naftaly and R. Dudley, "Terahertz reflectivities of metal-coated mirrors," *Appl. Opt.*, vol. 50, no. 19, pp. 3201–3204, Jul 2011. [Online]. Available: https://opg.optica.org/ao/abstract.cfm?URI=ao-50-19-3201

[22] L. Li, "New formulation of the fourier modal method for crossed surface-relief gratings," *J. Opt. Soc. Am. A*, vol. 14, no. 10, pp. 2758–2767, Oct 1997. [Online]. Available: https://opg.optica.org/josaa/abstract.cfm?URI=josaa-14-10-2758

[23] V. Liu and S. Fan, "S^4 : A free electromagnetic solver for layered periodic structures," *Computer Physics Communications*, vol. 183, no. 10, pp. 2233 – 2244, 2012. [Online]. Available: http://www.sciencedirect.com/science/article/pii/S0010465512001658

[24] G. Bao, Z. Chen, and H. Wu, "Adaptive finite-element method for diffraction gratings," *J. Opt. Soc. Am. A*, vol. 22, no. 6, pp. 1106–1114, Jun 2005. [Online]. Available: https://opg.optica.org/josaa/abstract.cfm?URI=josaa-22-6-1106

[25] D. C. O'Shea, T. J. Suleski, A. D. Kathman, and D. W. Prather, *Diffractive Optics: Design, Fabrication, and Test*. SPIE Press, 2004.